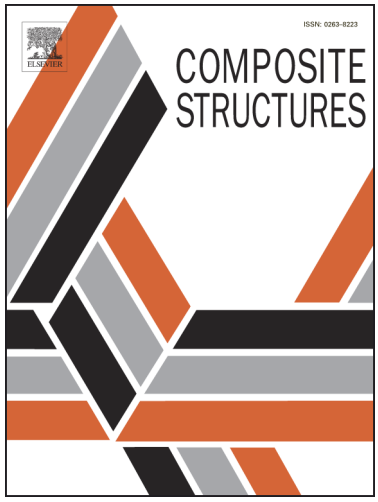

Geometrically Nonlinear Transient Analysis of Composite Laminated Plate and Shells Subjected to Low-Velocity Impact

Ik Hyeon Choi

PII: S0263-8223(16)00084-2
DOI: http://dx.doi.org/10.1016/j.compstruct.2016.01.070
Reference: COST 7176

To appear in: *Composite Structures*

Please cite this article as: Choi, I.H., Geometrically Nonlinear Transient Analysis of Composite Laminated Plate and Shells Subjected to Low-Velocity Impact, *Composite Structures* (2016), doi: http://dx.doi.org/10.1016/j.compstruct.2016.01.070

Geometrically Nonlinear Transient Analysis of Composite Laminated Plate and Shells Subjected to Low-Velocity Impact

Ik Hyeon Choi

Aerospace Application and Materials Research Team, Korea Aerospace Research Institute, South Korea

Abstract

In this study, the transient responses of a composite laminated plate and cylindrical shells subjected to low-velocity impacts were investigated numerically. The shear deformation theory of a doubly curved shell and von Karman's large deflection theory were used to develop a geometrically nonlinear finite element program. It is well-known that in the case of a flat plate with fixed boundary edges, a geometrically nonlinear analysis yields larger contact forces and smaller deflections than a corresponding linear analysis. However, in the case of cylindrical shells, an opposite result was found in this study; a geometrically nonlinear analysis exhibited smaller contact forces and larger deflections than a corresponding linear analysis. The reason for this opposite result is described in this study. Conversely, with a plate and shells that have the same size, shells with a larger curvature exhibited smaller deflections and larger contact forces. The strain distribution at the bottom surface of the plate/shells using the geometrically nonlinear analysis exhibited markedly or only marginally larger tensile areas than those produced using the linear analysis.

Keywords: geometrically nonlinear analysis, composite laminates, cylindrical shell, low-velocity impact, finite element program

E-mail address: ihchoi@kari.re.kr

1. Introduction

Many studies of the transient response and damage prediction of composite laminated flat plates subjected to low-velocity impacts have already been published [1]; authors have also presented certain papers on this field [2-9]. A geometrically nonlinear dynamic finite element program to analyse the impact response of composite laminated plates has been developed in references [2-4]. Generally, directly coding a finite element program to analyse impact response was not easy; thus, the author proposed a novel and simple method that could predict the approximate contact force history including its second-order fluctuations [5]. To use a general-purpose finite element code to analyse the impact response of laminated plates and sandwiches, the author proposed a new analytical method using a spring element and the linearized contact law concept [6, 7]. Generally, thin plates with in-plane pre-stress show different stiffnesses during out-of-plane deflections from the original plate without pre-stress. The author developed a new finite element formulation considering in-plane pre-strain and investigated the impact response of composite laminated plates with in-plane tensile and compressive pre-strain via numerical calculations and experimentation [8, 9]. In those studies, the author reported that in-plane tensile pre-strain increased the stiffness of a laminate during deflections caused by impacts, and in-plane compressive pre-strain could decrease the stiffness.

Recently, the impact response and damage of pressure vessels manufactured using composite material have been investigated in detail [10-12]. To accurately analyse the dynamic response and damage of pressurized vessels subjected to a drop impact or foreign object impact, we must consider the change in stiffness, which is described above, because the cylindrical wall of such a vessel is under in-plane pre-stress that is induced by the vessel's internal pressure. However, no analytical result that considers the change in stiffness has been identified to date. Thus, the author is in the process of developing a new finite element program that considers the change in the stiffness of a cylindrical shell structure experiencing in-plane pre-strain. However, in this preliminary study, a finite element program for the impact analysis of laminated curved shells without in-plane pre-stress was developed. In a subsequent study, the author will present the analytical result of the impact response of an in-plane pre-stressed cylinder wall caused by internal pressure.

Conversely, many studies in addition to the author's previous papers investigate the impact influence response of composite laminated flat plates. Based on those papers, geometrically nonlinear analysis that considers von Karman's large deflection theory produces larger contact forces and smaller deflections than a corresponding linear analysis because a geometrically nonlinear analysis can consider the membrane effect. The membrane effect describes how in-plane tensile deformations that are induced by the deflection of a flat plate due to an impact

influence can make the plate stiffer during the deflection. Such a membrane effect typically appears more strongly at plates with fixed boundary edges.

However, it is not well known what occurs if the von Karman's large deflection theory is considered in the analysis of composite laminated curved shells subjected to low-velocity impacts. Few papers consider the impact response of composite laminated curved shells [13-16]. Unfortunately, these studies don't provide much information regarding the abovementioned question. Thus, in this study, the author has developed an understanding on what phenomenon will occur in this case when von Karman's large deflection theory is applied to the analysis of the impact response of composite laminated curved shells, particularly cylindrically curved shells with all fixed boundary edges.

In summary, this study numerically examines the impact response of composite laminated plate and cylindrically curved shells with various curvatures and investigates geometrically nonlinear and linear analyses.

2. Geometrically Nonlinear Dynamic Finite Element Equation of a Composite Laminated Shell

A shear deformation theory of a doubly curved shell and von Karman's large deflection theory were used to develop a geometrically nonlinear finite element program. J. N. Reddy presented a finite element formulation for solving such a problem [17]. In this study, the same formulation was used to code the finite element program.

The strain-displacement relation of the shear deformation theory of a doubly curved shell and von Karman's large deflection theory is given by:

$$\varepsilon_1 = \varepsilon_1^0 + \zeta\,\kappa_1^0 = \frac{\partial u_1}{\partial x_1} + \frac{u_3}{R_1} + \frac{1}{2}\left(\frac{\partial u_3}{\partial x_1}\right)^2 + \zeta\,\frac{\partial \phi_1}{\partial x_1}$$

$$\varepsilon_2 = \varepsilon_2^0 + \zeta\,\kappa_2^0 = \frac{\partial u_2}{\partial x_2} + \frac{u_3}{R_2} + \frac{1}{2}\left(\frac{\partial u_3}{\partial x_2}\right)^2 + \zeta\,\frac{\partial \phi_2}{\partial x_2}$$

$$\varepsilon_6 = \varepsilon_6^0 + \zeta\,\kappa_6^0 = \frac{\partial u_2}{\partial x_1} + \frac{\partial u_1}{\partial x_2} + \frac{\partial u_3}{\partial x_1}\frac{\partial u_3}{\partial x_2} + \zeta\left(\frac{\partial \phi_2}{\partial x_1} + \frac{\partial \phi_1}{\partial x_2} + c_0\left(\frac{\partial u_2}{\partial x_1} - \frac{\partial u_1}{\partial x_2}\right)\right) \quad (1)$$

$$\varepsilon_4 = \varepsilon_4^0 = \frac{\partial u_3}{\partial x_2} + \phi_2 - \frac{u_2}{R_2}$$

$$\varepsilon_5 = \varepsilon_5^0 = \frac{\partial u_3}{\partial x_1} + \phi_1 - \frac{u_1}{R_1}$$

where:

$$c_0 = \frac{1}{2}\left(\frac{1}{R_2} - \frac{1}{R_1}\right)$$

Hamilton's principle, which is the principle of virtual work including dynamic behaviour can be written as:

$$\begin{aligned} 0 = \int_\Omega [\, & N_1\delta\varepsilon_1^0 + N_2\delta\varepsilon_2^0 + N_6\delta\varepsilon_6^0 + M_1\delta\kappa_1^0 + M_2\delta\kappa_2^0 + M_6\delta\kappa_6^0 + Q_1\delta\varepsilon_5^0 + Q_2\delta\varepsilon_4^0 \\ & + \left(P_1\ddot{u}_1 + P_2\ddot{\phi}_1\right)\delta u_1 + \left(\overline{P}_1\ddot{u}_2 + \overline{P}_2\ddot{\phi}_2\right)\delta u_2 + I_1\ddot{u}_3\delta u_3 \\ & + \left(I_3\ddot{\phi}_1 + P_2\ddot{u}_1\right)\delta\phi_1 + \left(I_3\ddot{\phi}_2 + \overline{P}_2\ddot{u}_2\right)\delta\phi_2 - q\delta u_3]\alpha_1\alpha_2 d\xi_1 d\xi_2 \end{aligned} \quad (2)$$

where:

$$P_1 = I_1 + \frac{2I_2}{R_1}, \quad P_2 = I_2 + \frac{I_3}{R_1}, \quad \overline{P}_1 = I_1 + \frac{2I_2}{R_2}, \quad \overline{P}_2 = I_2 + \frac{I_3}{R_2} \quad (3)$$

The meaning of each term and notation in equation (2) is described in J. N. Reddy's paper [17]. Equation (2) can be used to derive the following finite element equation (4), which can be used for the dynamic analysis of a composite laminated plate or curved shell. The detailed mass and stiffness matrices can be found in J. N. Reddy's paper and in the Appendix of this paper because a typing error was found in J. N. Reddy's paper in one term of the stiffness matrices, $[K_L^{23}]$:

$$[M]\{\ddot{U}\} + \left[[K_L] + [K_N\{U\}]\right]\{U\} = \{F\} \quad (4)$$

Conversely, an impactor was assumed to be a point mass; thus, the dynamic equation for the impactor can be written as equation (5). The two dynamic equations for the plate/shell and impactor were calculated simultaneously using the modified Hertzian contact law (6). The detailed solving procedure for the three equations and the meaning of each term and notation in equations (5) and (6) can be found in the author's other studies [2-6]:

$$m\ddot{u}_3 + F = 0 \tag{5}$$

$$F = k\alpha^n, \text{ where } k = \frac{4}{3}\frac{R^{1/2}}{(1-\nu_r^2)/E_r + 1/E_p} \tag{6}$$

All of the laminated composite plate/shells considered in this study had the same dimension of 31.4 x 31.4 x 0.228 cm, where the dimension indicates the curved length in the case of a curved shell. The stacking sequence of the plate/shells is $[90/0]_{4S}$. As shown in Fig. 1, the plate/shells were assumed to be impacted at the centre by a steel impactor with a contacting spherical cap with a radius of 0.635 cm, which was used as the value of R in the modified Hertzian contact law of equation (6). The stacking sequence of the laminates only included 0° and 90° (i.e., there is no angle ply like ±30° or ±45°). Thus, only a quarter of the plate/shells can be meshed and calculated, as shown in Fig. 1.

As described in Fig. 1, all of the boundary edges of the plate/shells subjected to the low-velocity impact were assumed to be fixed. The curvature in the x_2-coordinate was zero, and the curvature in the x_1-coordinate had a given value between zero (i.e., a flat plate) and a maximum value (i.e., a complete cylinder).

The elastic properties of a graphite/epoxy lamina were assumed to be as follows:

E_1 = 129 GPa, E_2 = 8.1 GPa, ν_{12} = 0.31, ν_{23} = 0.52,

$G_{12} = G_{13}$ = 3.59 GPa, G_{23} = 1.87 GPa, $\rho = 1.58 \times 10^{-5}$ N s^2/cm^4

The impact condition considered in this study included a impactor mass of 1.366 kg and an impact velocity of 3.61 m/s; thus, the impact energy was approximately 8.9 J.

The finite element used in this program is a nine-node iso-parametric plate element. To check for convergence on the mesh size, meshes between 4 x 4 and 24 x 24 for a quarter of the plate/shell was tested; a fine mesh great than 12 x 12 was found to be sufficient for convergence. Thus, in this study, a 16 x 16 mesh was selected for use. Another convergence of the dynamic solution was checked with a varying time interval from 10 to 160 μsec. An time interval of less than 80 μsec always produced good convergence, and thus, 40 μsec was selected for use in this study. The author also checked what different results were derived between the full integration method and the reduced integration method for the calculation of the inter-laminar shear stiffness

matrices. Reduced integration of the inter-laminar shear stiffness matrices showed faster convergence than the full integration method; however, it produced divergent contact forces in certain cases, even with a fine mesh near 16 x 16; thus, the full integration method was used in this study.

3. Results and Review

Fig. 2 shows the deformed meshes of composite laminated plate/shells when a deflection due to an impact (i.e., a central deflection) reached is maximum value, which was calculated via geometrically nonlinear analysis. Fig. 3 shows the undeformed and deformed cross sectional curves along the x_1 axis (i.e., x_2=0) of the composite laminated plate/shells subjected to a low-velocity impact, which were calculated via geometrically nonlinear and linear analysis. Fig. 4 shows the overlapped curves of the deformed cross sectional curves along the x_1 axis (i.e., x_2=0) of the composite laminated plate/shells.

In the figures, the deflections in the thickness direction were exaggerated by a magnification of five times to easily distinguish the deformed shapes. From the figures, it is shown that the larger curvature exhibited smaller deflections; a larger resistance to deflection is evident in a curved shell with a larger curvature because the two curved sides along the x_1 axis of the shell support a given portion of the vertical directional contact force similar pillars supporting a bridge. In addition, a shell with a larger curvature has a shorter portion of its structure that corresponds to the top of a bridge; thus, the resistive property of the specimen to the deflection of the curved shell should be higher.

The above interpretation is based on the geometric shape of the cylindrical shell. In addition, it can also be interpreted more theoretically. In the Appendix, certain terms including the radii (R_1 and R_2) of the curved shell are present in the stiffness matrices, particularly $[\mathrm{K}_{\mathrm{L}}^{33}]$ and $[\mathrm{K}_{\mathrm{N}}^{33}]$. The upper index (33) in the matrix terms indicates the stiffness to displacement in the thickness direction (i.e., deflection) induced by a force in the thickness directional (i.e., a contact force). If a cylindrically curved shell has a larger curvature, a matrix with an index of 33 should be larger due to the smaller radius, R_1; thus, a shell with a larger curvature should show a smaller deflection.

Fig. 5 shows the central deflection (i.e., the deflection of the impacted position) histories of the composite laminated plate/shells subjected to low-velocity impacts. Fig. 6 shows the contact force histories of the composite laminated plate/shells. From Figs. 3 through 6, it is shown that geometrically nonlinear analysis produces smaller deflections and larger contact forces than the corresponding linear analysis in the case of a composite laminated flat plate with fixed boundary edges; this is a well-known phenomenon that can be found in many studies, including the author's other studies.

However, in the case of cylindrically curved shells, a phenomenon that is opposite to that produced by the geometrically nonlinear analysis exhibits larger deflections and smaller contact forces than the corresponding linear analysis, even though the specimen has fixed boundary edges. Generally, when we want to obtain more accurate results in the response analysis of a

plate/shell, we consider the von Karman's large deflection theory, which considers in-plane tensile/compressive displacements that are induced by out-of-plane deflections of the plate/shell. The calculation of the in-plane tensile/compressive displacements in a geometrically nonlinear analysis indicates the calculation of different deflections from the corresponding linear analysis.

In the case of a flat plate, in-plane tensile displacement induced by deflection increases the resistance of the specimen during deflection (i.e., stiffening effect), where the tensile displacement is induced primarily due to the fixed boundary condition of the plate/shell. However, in the case of a curved shell, even though it has fixed boundary condition, in-plane compressive displacement is induced by deflection due to the geometric characteristics of its curved shape; it thus exhibits increasing amounts of deflection (i.e., softening effect). The deflection of a shell induces the shell to be compressed in the in-plane direction, and the induced compressive displacement finally produces a marginally larger deflection of the shell. Generally, with the same impact condition, a larger deflection indicates a larger contact duration, and a larger contact duration indicates a smaller contact force based on the impulse-momentum conservative theory. In summary, in the case of a curved shell, the membrane effect is reversed.

From Figs. 4 to 5, it is shown that the plate/shells with larger curvatures exhibit smaller deflections in sequence. However, in Fig. 6, it is shown that only the curved shells, not including the flat plate, with larger curvatures exhibited higher contact forces in sequence. This appears to be an exceptional phenomenon, where the flat plate shows a higher contact force than the curved shells with R_1 = 10 and 20. It can be estimated that the flat plate had a considerably softer stiffness during deflection; thus, the magnitude of the second-order fluctuation in the contact force history curve was large compared to that of the first-order fluctuation. Then, the peak value of the contact force history of the flat plate became markedly higher via superposition of the two fluctuations. This type of characteristic on the fluctuation of the contact force history curve is described in the author's other study [5].

Figs. 7 and 8 show the x_1- and x_2-directional strain distributions at the bottom surface of a quarter of the composite laminated plate/shells, which were obtained from the geometrically nonlinear analysis and the linear analysis. In the figures, a thick solid line indicates zero strain; a thin solid line indicates a tensile strain; and a thin dashed line indicates a compressive strain. The contour interval shown is 1,000 μ-strain. From the figures, it is shown that in the case of flat plate, a large difference between the two analyses is shown. The linear analysis shows that nearly half of the plate was in tensile strain area, and the other half was in compressive strain area; however, the geometrically nonlinear analysis shows that nearly all of the area of the plate was in tensile strain area. This large difference between the two analyses indicates that it is necessary to apply von Karman's large deflection theory, particularly in the case of a flat plate.

However, in the case of curved shells, the two analyses showed relatively small differences, which could have been caused primarily near the impact location. However, these small differences may be important when accurately predicting the impact's damage area because small differences in the strain components may estimate different sizes of the damaged area.

Conversely, even though certain displacement components are considerably different between the two analyses, the numerically calculated strain values are similar; this occurs because the displacement terms that create the strain component are different between the geometrically nonlinear analysis and linear analysis. In equation (1), the detailed displacement terms that construct the strain components for the geometrically nonlinear analysis are shown; if the three terms, $\frac{1}{2}\left(\frac{\partial u_3}{\partial x_1}\right)^2$, $\frac{1}{2}\left(\frac{\partial u_3}{\partial x_2}\right)^2$ and $\frac{\partial u_3}{\partial x_1}\frac{\partial u_3}{\partial x_2}$ are ignored in equation (1), we obtain the strain-displacement relation for the linear analysis. Because the strain components were constructed differently in the two analyses, the strain components can be similar, even though the displacement values in the two analyses are different.

4. Conclusions

In this study, the transient responses of composite laminated plate and cylindrical shells subjected to low-velocity impacts were investigated numerically. In the case of a flat plate with fixed boundary edges, the geometrically nonlinear analysis showed larger contact forces and smaller deflections than the corresponding linear analysis. However, in the case of cylindrical shells, it showed an opposite result: the geometrically nonlinear analysis showed marginally smaller contact forces and marginally larger deflections than the corresponding linear analysis; this occurs because the deflection of the curved shell induces an in-plane compressive displacement, which produces a marginally larger deflection. In summary, the membrane effect appears to be reversed in the case of a curved shell.

The plate/shells with larger curvatures consistently exhibited smaller deflections. The curved shells, not including the flat plate, with larger curvatures also consistently showed larger contact forces. However, the flat plate showed a larger peak value in the contact force history than the curved shells with R_1=20 or 10 due to superposition of certain fluctuations. The strain distribution at the bottom surface of the flat plate produced by the geometrically nonlinear analysis exhibited a large difference from that produced by the linear analysis; however, the strain distributions of the curved shells showed relatively small differences between the two analyses. Although this different is small in the curved shells, a geometrically nonlinear analysis should be performed to obtain a more accurate strain field for more accurate predictions of the impact damage area.

Reference

[1] Abrate S. Modeling of impacts on composite structures. Compos Struct 2001;51:129–38.

[2] Choi IH, Hong CS. Low-velocity impact response of composite laminates considering higher-order shear deformation and large deflection. Mech Compos Mater Struct 1994;1:157–70.

[3] Choi IH. Response and damage of composite laminates subjected to low velocity impact. PhD thesis, Korea Advanced Institute of Science and Technology, 1994.

[4] Hong CS, Choi IH, Kim CG. Estimation of damage area due to low-velocity impact in composite laminate. In: 9th Technical conference proceeding of the American Society for Composites 1994; 473–81.

[5] Choi IH, Hong CS. New approach for simple prediction of impact force history on composite laminates. AIAA J 1994;32(10):2067–72.

[6] Choi IH, Lim CH. Low-velocity impact analysis of composite laminates using linearized contact law. Compos Struct 2004;66:125–32.

[7] Choi IH. Contact force history analysis of composite sandwich plates subjected to low-velocity impact. Compos Struct 2006;75:582–6.

[8] Choi IH. Low-velocity impact analysis of composite laminates under initial in-plane load. Compos Struct 2008;86:251–7.

[9] Choi IH, Kim IG, Ahn SM, Yeom CH. Analytical and experimental studies on the low-velocity impact response and damage of composite laminates under in-plane loads with structural damping effects. Compos Sci Technol 2010;70:1513–22.

[10] Changliang Z, Mingfa R, Wei Z, Haoran C. Delamination prediction of composite filament wound vessel with metal liner under low velocity impact. Compos Struct 2006;75:387-92.

[11] Perillo G, Grytten F, Sørbø S, Delhaye V. Numerical/experimental impact events on filament wound composite pressure vessel. Compos: Part B 2015;69:406–17.

[12] Han MG, Chang SH. Failure analysis of a Type III hydrogen pressure vessel under impact loading induced by free fall. Compos Struct 2015;127:288–97.

[13] Kim SJ, Goo NS, Kim TW. The effect of curvature on the dynamic response and impact-induced damage in composite laminates. Compos Sci Technol 1997;763–73.

[14] Ganapathy S, Rao KP. Failure analysis of laminated composite cylindrical/spherical shell panels subjected to low-velocity impact. Comut Struct 1998;68:627–41.

[15] Her SC, Liang YC. The finite element analysis of composite laminates and shell structures subjected to low velocity impact. Compos Struct 2004;66:277–85.

[16] Zhao GP, Cho CD. Damage initiation and propagation in composite shells subjected to impact. Compos Struct 2007;78:91–100.

[17] Reddy JN, Chandrashekhara K. Geometrically non-linear transient analysis of laminated, doubly curved shells. Int J Non-linear Mech 1985;20(2):79–90.

APPENDIX

The mass and stiffness matrices are written as:

$$[M]=\begin{bmatrix} P_1[S^{00}] & 0 & 0 & P_2[S^{00}] & 0 \\ & \overline{P}_1[S^{00}] & 0 & 0 & \overline{P}_2[S^{00}] \\ & & I_1[S^{00}] & 0 & 0 \\ & sym. & & I_3[S^{00}] & 0 \\ & & & & I_3[S^{00}] \end{bmatrix}$$

$$[K_L]=\begin{bmatrix} [K_L^{11}] & [K_L^{12}] & [K_L^{13}] & [K_L^{14}] & [K_L^{15}] \\ & [K_L^{22}] & [K_L^{23}] & [K_L^{24}] & [K_L^{25}] \\ & & [K_L^{33}] & [K_L^{34}] & [K_L^{35}] \\ & sym. & & [K_L^{44}] & [K_L^{45}] \\ & & & & [K_L^{55}] \end{bmatrix}$$

$$[K_N]=\begin{bmatrix} 0 & 0 & [K_N^{13}] & 0 & 0 \\ 0 & 0 & [K_N^{23}] & 0 & 0 \\ [K_N^{31}] & [K_N^{32}] & [K_N^{33}] & [K_N^{34}] & [K_N^{35}] \\ 0 & 0 & [K_N^{43}] & 0 & 0 \\ 0 & 0 & [K_N^{53}] & 0 & 0 \end{bmatrix}$$

The mass coefficients are written as:

$[M^{11}]=P_1[S^{00}]$, $[M^{14}]=P_2[S^{00}]$, $[M^{22}]=\overline{P}_1[S^{00}]$, $[M^{25}]=\overline{P}_2[S^{00}]$

$[M^{41}]=[M^{14}]$, $[M^{52}]=[M^{25}]$, $[M^{33}]=I_1[S^{00}]$, $[M^{44}]=[M^{55}]=I_3[S^{00}]$, all other $[M^{\alpha\beta}]=0$

The linear stiffness coefficients are written as:

$$[K_L^{11}]=A_{11}[S^{11}]+A_{16}([S^{12}]+[S^{21}])+A_{66}[S^{22}]$$

$$-c_0(B_{16}([S^{12}]+[S^{21}])+2B_{66}[S^{22}]-c_0D_{66}[S^{22}])+\frac{A_{55}}{R_1^2}[S^{00}]$$

$$[K_L^{12}]=A_{12}[S^{12}]+A_{16}[S^{11}]+A_{26}[S^{22}]+A_{66}[S^{21}]$$

$$-c_0(B_{26}[S^{22}]-B_{16}[S^{11}]+c_0D_{66}[S^{21}])+\frac{A_{45}}{R_1R_2}[S^{00}]$$

$$[K_L^{13}]=\frac{1}{R_1}(A_{11}[S^{10}]+A_{16}[S^{20}])+\frac{1}{R_2}(A_{12}[S^{10}]+A_{26}[S^{20}])$$

$$-c_0(\frac{B_{16}}{R_1}[S^{20}]+\frac{B_{26}}{R_2}[S^{20}])-\frac{1}{R_1}(A_{45}[S^{02}]+A_{55}[S^{01}])$$

$$[K_L^{14}]=B_{11}[S^{11}]+B_{16}([S^{12}]+[S^{21}])+B_{66}[S^{22}]-c_0(D_{16}[S^{21}]+D_{66}[S^{22}])-\frac{1}{R_1}A_{55}[S^{00}]$$

$$[K_L^{15}]=B_{12}[S^{12}]+B_{16}[S^{11}]+B_{26}[S^{22}]+B_{66}[S^{21}]-c_0(D_{26}[S^{22}]+D_{66}[S^{21}])-\frac{1}{R_1}A_{45}[S^{00}]$$

$$[K_L^{22}]=A_{22}[S^{22}]+A_{26}\left([S^{12}]+[S^{21}]\right)+A_{66}[S^{11}]+2c_0B_{66}[S^{11}]$$

$$+c_0(B_{26}([S^{12}]+[S^{21}])+c_0D_{66}[S^{11}])+\frac{A_{44}}{R_2^{\ 2}}[S^{00}]$$

$$[K_L^{23}]=\frac{1}{R_1}(A_{12}[S^{20}]+A_{16}[S^{10}])+\frac{1}{R_2}(A_{22}[S^{20}]+A_{26}[S^{10}])$$

$$+c_0\left(\frac{B_{16}}{R_1}+\frac{B_{26}}{R_2}\right)[S^{10}]-\frac{1}{R_2}(A_{44}[S^{02}]+A_{45}[S^{01}])$$

$$[K_L^{24}]=B_{12}[S^{21}]+B_{26}[S^{22}]+B_{16}[S^{11}]+B_{66}[S^{12}]+c_0(D_{16}[S^{11}]+D_{66}[S^{12}])-\frac{1}{R_2}A_{45}[S^{00}]$$

$$[K_L^{25}]=B_{22}[S^{22}]+B_{26}([S^{21}]+[S^{12}])+B_{66}[S^{11}]+c_0(D_{26}[S^{12}]+D_{66}[S^{11}])-\frac{1}{R_2}A_{44}[S^{00}]$$

$$[K_L^{33}]=A_{45}[S^{12}]+A_{55}[S^{11}]+A_{44}[S^{22}]+A_{45}[S^{21}]+[S^{00}]\left[\frac{1}{R_1}\left(\frac{A_{11}}{R_1}+\frac{A_{12}}{R_2}\right)+\frac{1}{R_2}\left(\frac{A_{12}}{R_1}+\frac{A_{22}}{R_2}\right)\right]$$

$$[K_L^{34}]=A_{55}[S^{10}]+A_{45}[S^{20}]+\left(\frac{B_{11}}{R_1}+\frac{B_{12}}{R_2}\right)[S^{01}]+\left(\frac{B_{16}}{R_1}+\frac{B_{26}}{R_2}\right)[S^{02}]$$

$$[K_L^{35}]=A_{45}[S^{10}]+A_{44}[S^{20}]+\left(\frac{B_{16}}{R_1}+\frac{B_{26}}{R_2}\right)[S^{01}]+\left(\frac{B_{12}}{R_1}+\frac{B_{22}}{R_2}\right)[S^{02}]$$

$$[K_L^{44}]=D_{11}[S^{11}]+D_{16}([S^{12}]+[S^{21}])+D_{66}[S^{22}]+A_{55}[S^{00}]$$

$$[K_L^{45}]=D_{12}[S^{12}]+D_{16}[S^{11}]+D_{26}[S^{22}])+D_{66}[S^{21}]+A_{45}[S^{00}]$$

$$[K_L^{55}]=D_{22}[S^{22}]+D_{26}([S^{12}]+[S^{21}])+D_{66}[S^{11}]+A_{44}[S^{00}]$$

$[K_L^{\alpha\beta}]=[K_L^{\beta\alpha}]^T$ for $\alpha\beta$=21, 31, 32, 41, 42, 43, 51, 52, 53, 54

The nonlinear stiffness coefficients are written as:

$$[K_{NL}^{13}]=f_1(A_{11}[S^{11}]+A_{16}([S^{12}]+[S^{21}])+A_{66}[S^{22}])+f_2(A_{12}[S^{12}]+A_{16}[S^{11}]+A_{26}[S^{22}]+A_{66}[S^{21}])$$

$$-c_0[f_1(B_{16}[S^{21}]+B_{66}[S^{22}])+f_2(B_{26}[S^{22}]+B_{66}[S^{21}])]$$

$$[K_{NL}^{23}]=f_1(A_{12}[S^{21}]+A_{26}[S^{22}]+A_{16}[S^{11}]+A_{66}[S^{12}])+f_2(A_{22}[S^{22}]+A_{26}\left([S^{21}]+[S^{12}]\right)+A_{66}[S^{11}])$$

$$+c_0[f_1\left(B_{16}[S^{11}]+B_{66}[S^{12}]\right)+f_2\left(B_{26}[S^{12}]+B_{66}[S^{11}]\right)]$$

$$[K_{NL}^{33}]=2[S^{11}]\left(A_{11}f_1^2+2A_{16}f_1f_2+A_{12}f_2^2\right)+2([S^{12}]+[S^{21}])[f_1^2A_{16}+2A_{66}f_1f_2+f_2^2A_{26}]$$

$$+2[S^{22}](A_{12}f_1^2+2A_{26}f_1f_2+A_{22}f_2^2)$$

$$+([S^{01}]+2[S^{10}])\left[f_1\left(\frac{A_{11}}{R_1}+\frac{A_{12}}{R_2}\right)+f_2\left(\frac{A_{16}}{R_1}+\frac{A_{26}}{R_2}\right)\right]$$

$$+([S^{02}]+2[S^{20}])\left[f_1\left(\frac{A_{16}}{R_1}+\frac{A_{26}}{R_2}\right)+f_2\left(\frac{A_{12}}{R_1}+\frac{A_{22}}{R_2}\right)\right]$$

$$[K_{NL}^{34}]=2f_1(B_{11}[S^{11}]+B_{16}([S^{12}]+[S^{21}])+B_{66}[S^{22}])$$

$$+2f_2(B_{12}[S^{21}]+B_{66}[S^{12}]+B_{26}[S^{22}]+B_{16}[S^{11}])$$

$$[K_{NL}^{35}]=2f_1(B_{12}[S^{12}]+B_{66}[S^{21}]+B_{16}[S^{11}]+B_{26}[S^{22}])$$

$$+2f_2\left(B_{22}[S^{22}]+B_{26}([S^{12}]+[S^{21}])+B_{66}[S^{11}]\right)$$

$$[K_{NL}^{\alpha\beta}]=2[K_{NL}^{\beta\alpha}]^T \quad \text{for} \quad \alpha\beta=31,\ 32,\ 34,\ 35\,, \text{ all other } [K_{NL}^{\alpha\beta}]=0$$

where:

$$f_1=\frac{1}{2}\frac{\partial u_3}{\partial x_1},\quad f_2=\frac{1}{2}\frac{\partial u_3}{\partial x_2}$$

$$c_0=\frac{1}{2}\left(\frac{1}{R_2}-\frac{1}{R_1}\right)$$

$$P_i^{\alpha}=\int_{\Omega^e}\frac{\partial\psi_i}{\partial x_\alpha}dx_1dx_2\,,\qquad P_i^0=\int_{\Omega^e}\psi_i dx_1dx_2$$

$$S_{ij}^{\alpha\beta}=\int_{\Omega^e}\frac{\partial\psi_i}{\partial x_\alpha}\frac{\partial\psi_j}{\partial x_\beta}dx_1dx_2,\qquad S_{ij}^{00}=\int_{\Omega^e}\psi_i\psi_j dx_1dx_2$$

$$\int_{\Omega^e}f_1A_{11}\psi_i\psi_j dx_1dx_2=\sum_{I=1}^{N}\sum_{J=1}^{N}A_{11}\left[\left(\frac{\partial u_3}{\partial x_1}\right)\psi_i\psi_j\right]_{x_1=Z_I,x_2=Z_J}W_IW_J\det J_0$$

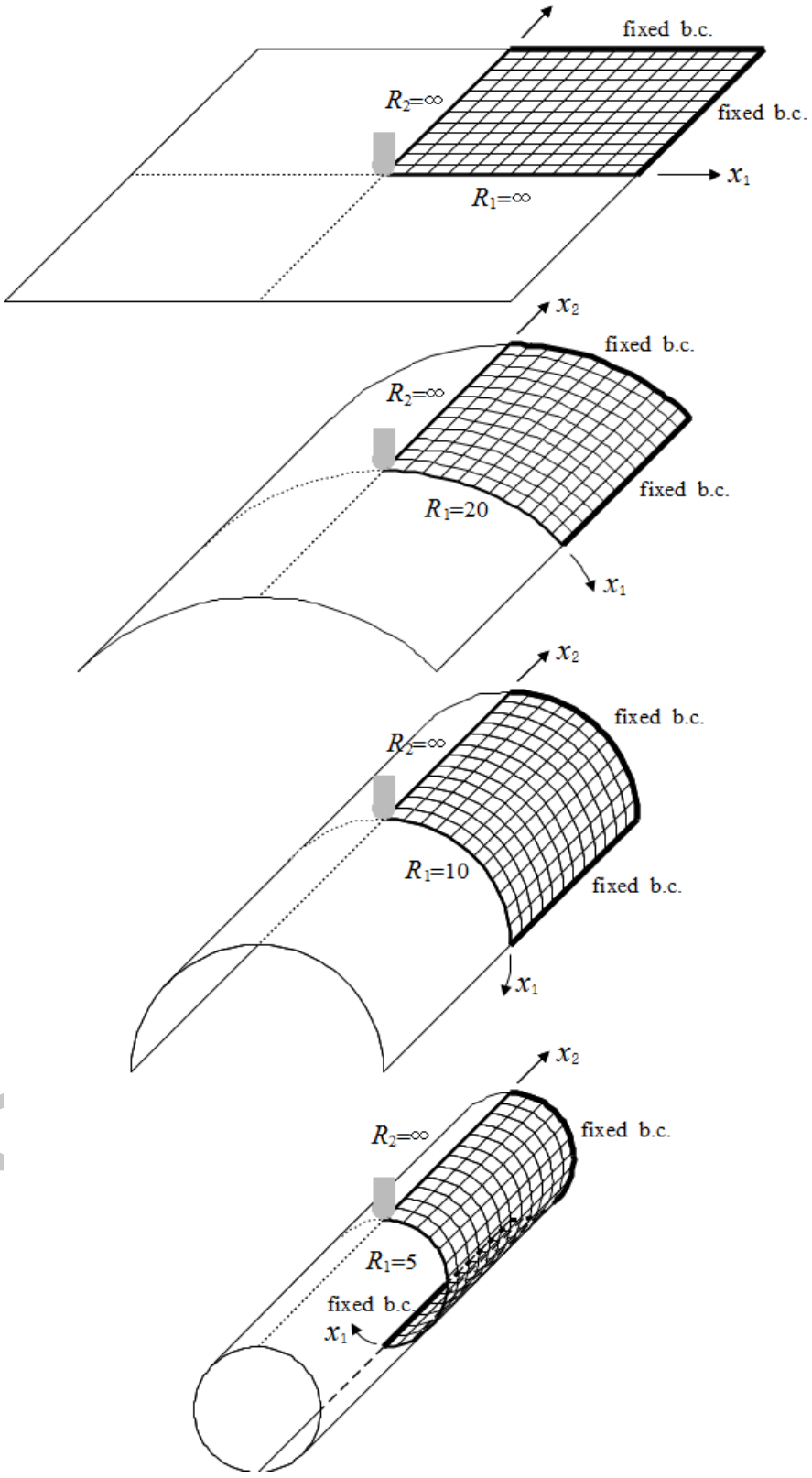

Fig. 1 Finite element meshes of composite laminated plate/shells with various curvatures.

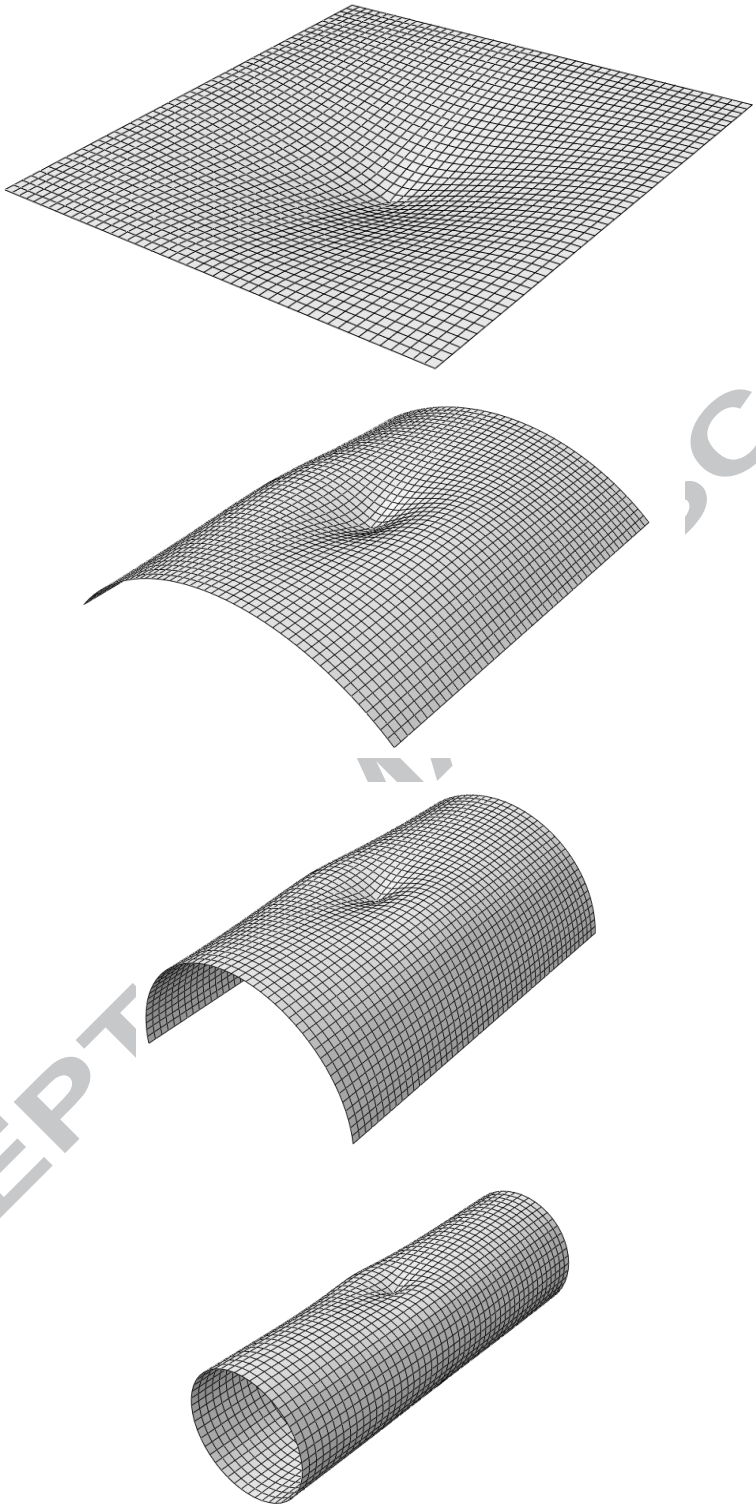

*Deformation in thickness direction was magnified by five times.

Fig. 2 Deformed meshes of composite laminated plate/shells calculated by geometrically nonlinear analysis.

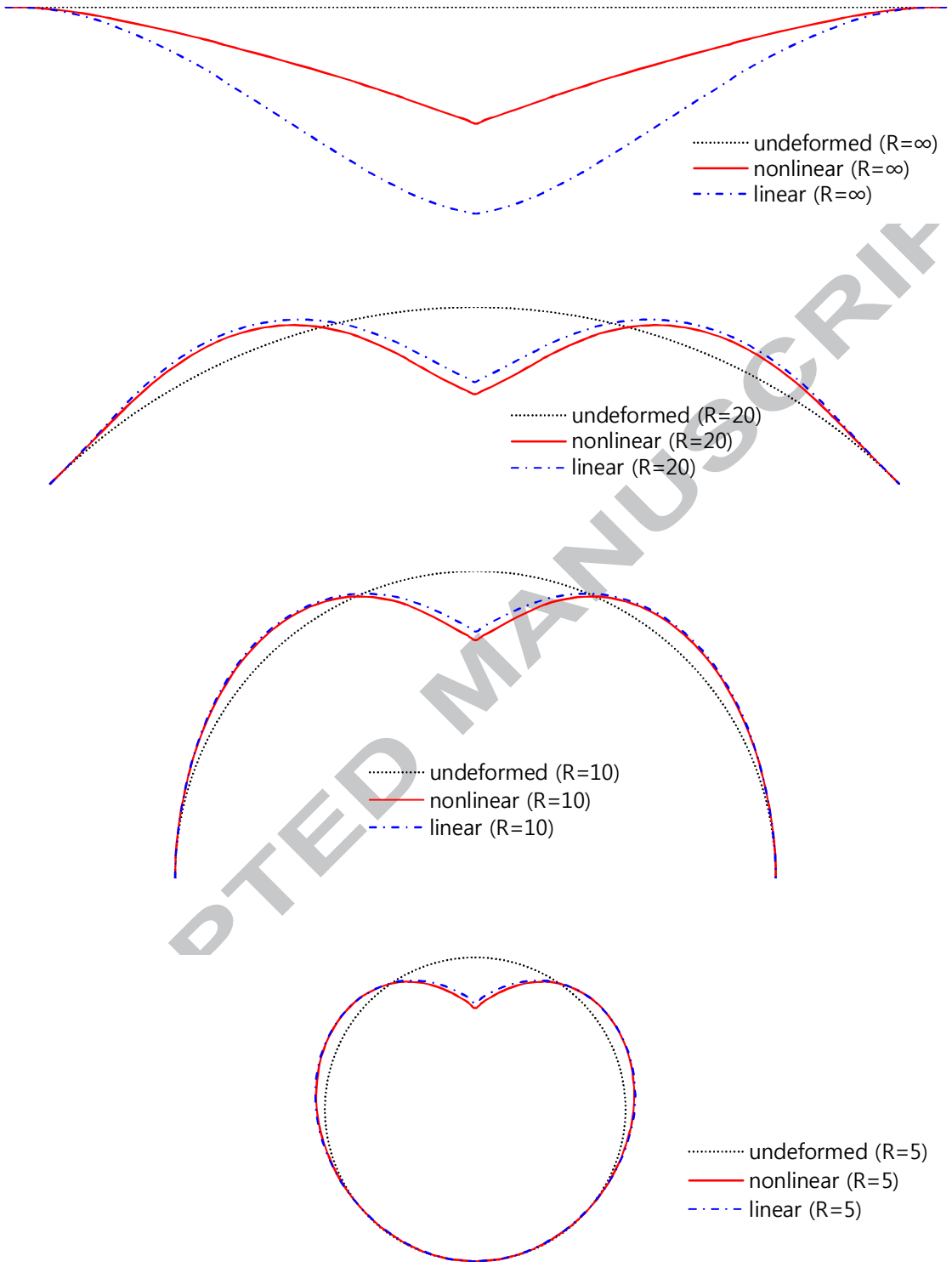

*Deformation in thickness direction was magnified by five times.

Fig. 3 Undeformed and deformed cross sectional curves along x_1 axis (x_2=0) of composite laminated plate/shells.

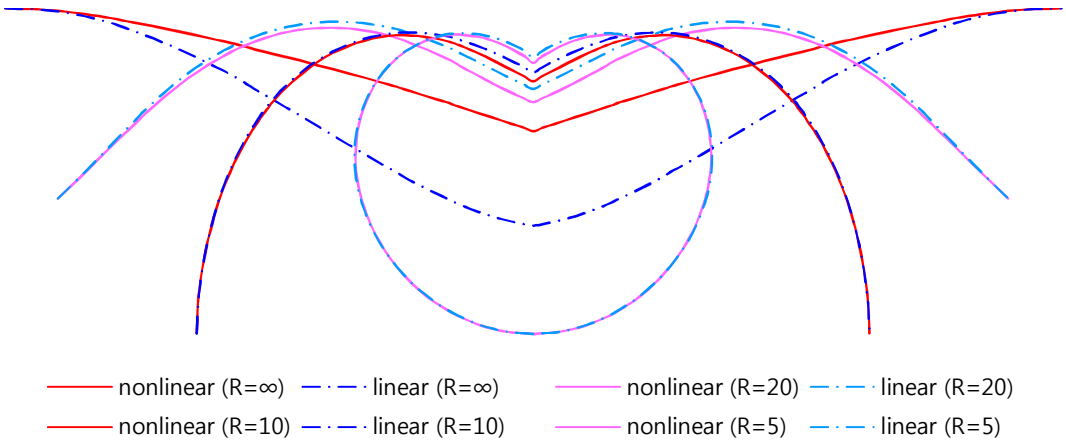

**Deformation in thickness direction was magnified by five times.*

Fig. 4 Overlapped deformed cross sectional curves along x_1 axis (x_2=0) of composite laminated plate/shells.

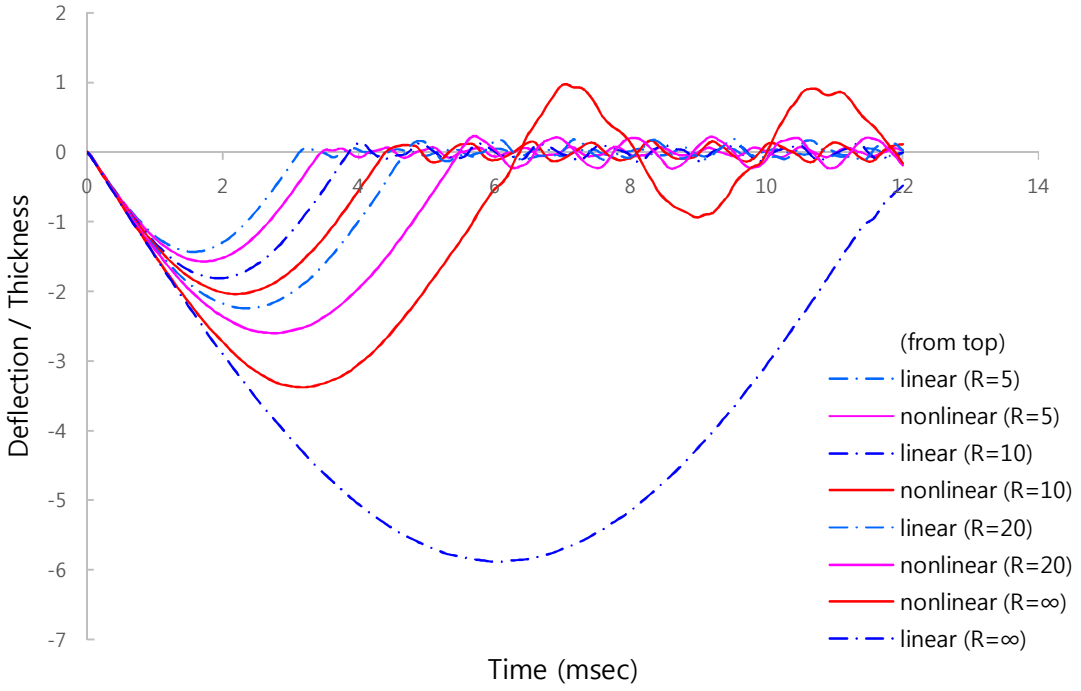

Fig. 5 Central deflection histories of composite laminated plate/shells.

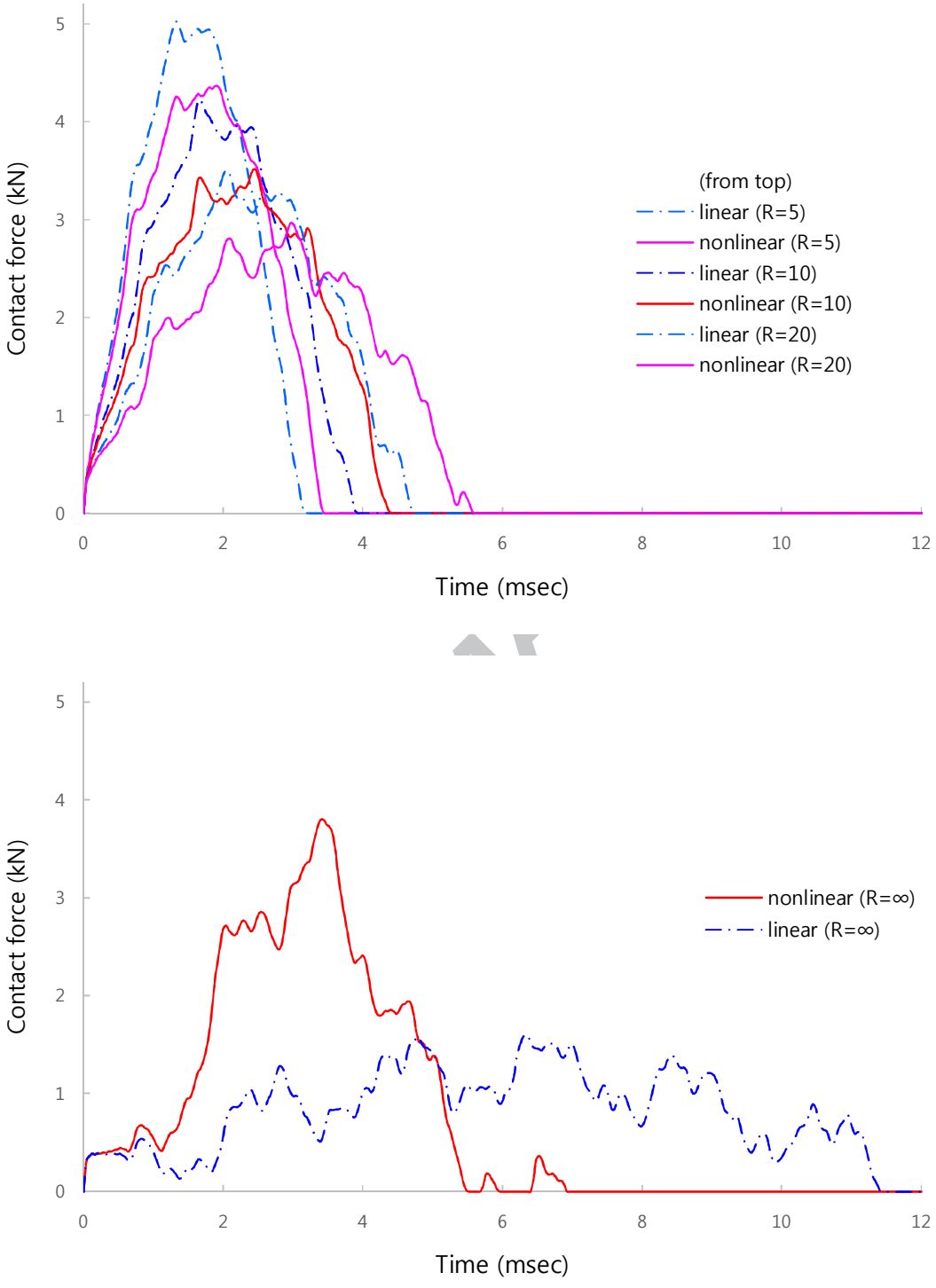

Fig. 6 Contact force histories of composite laminated plate/shells.

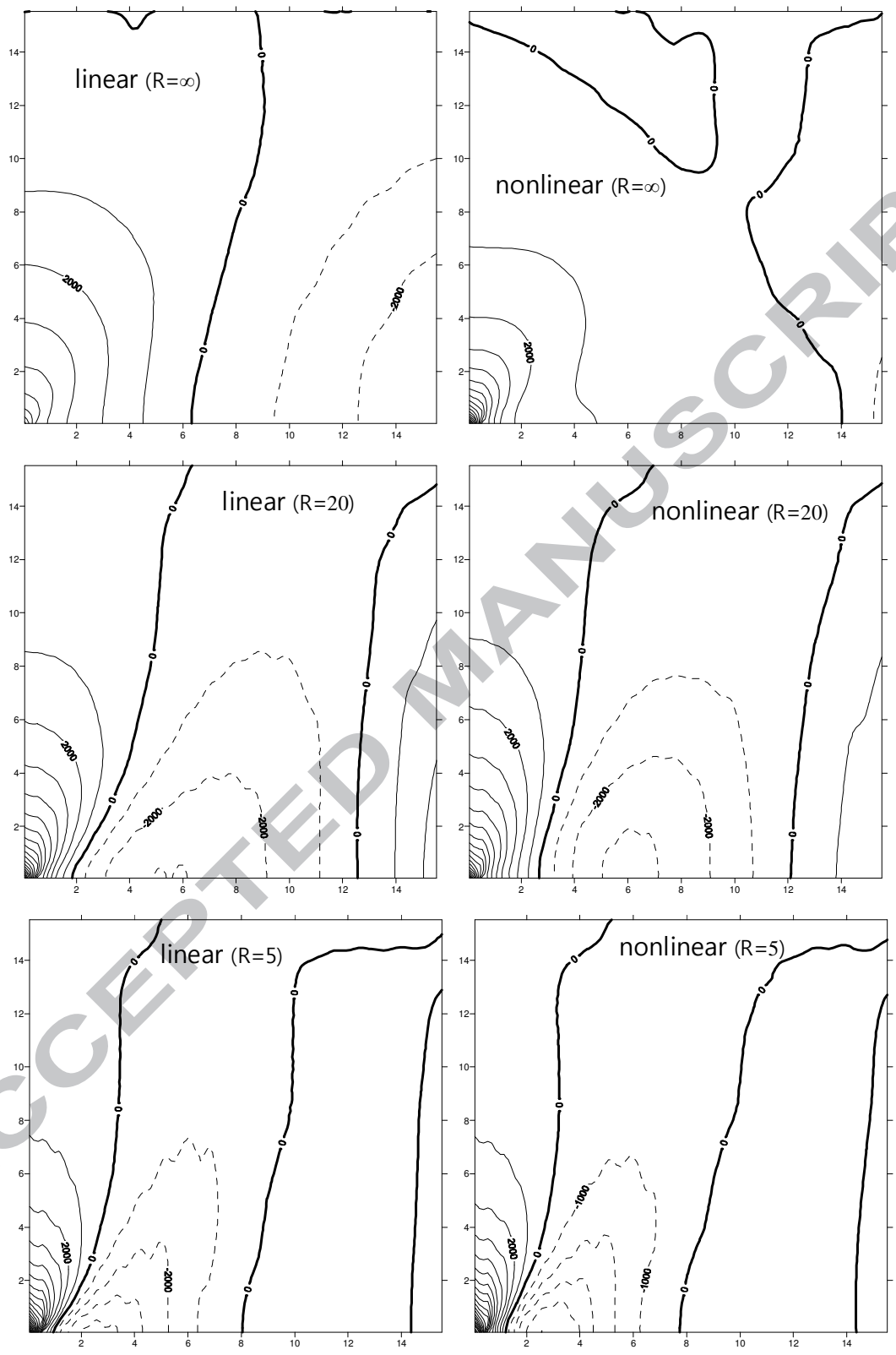

Fig. 7 X_1-directional strain distributions at bottom surface of a quarter part of composite laminated plate/shells.

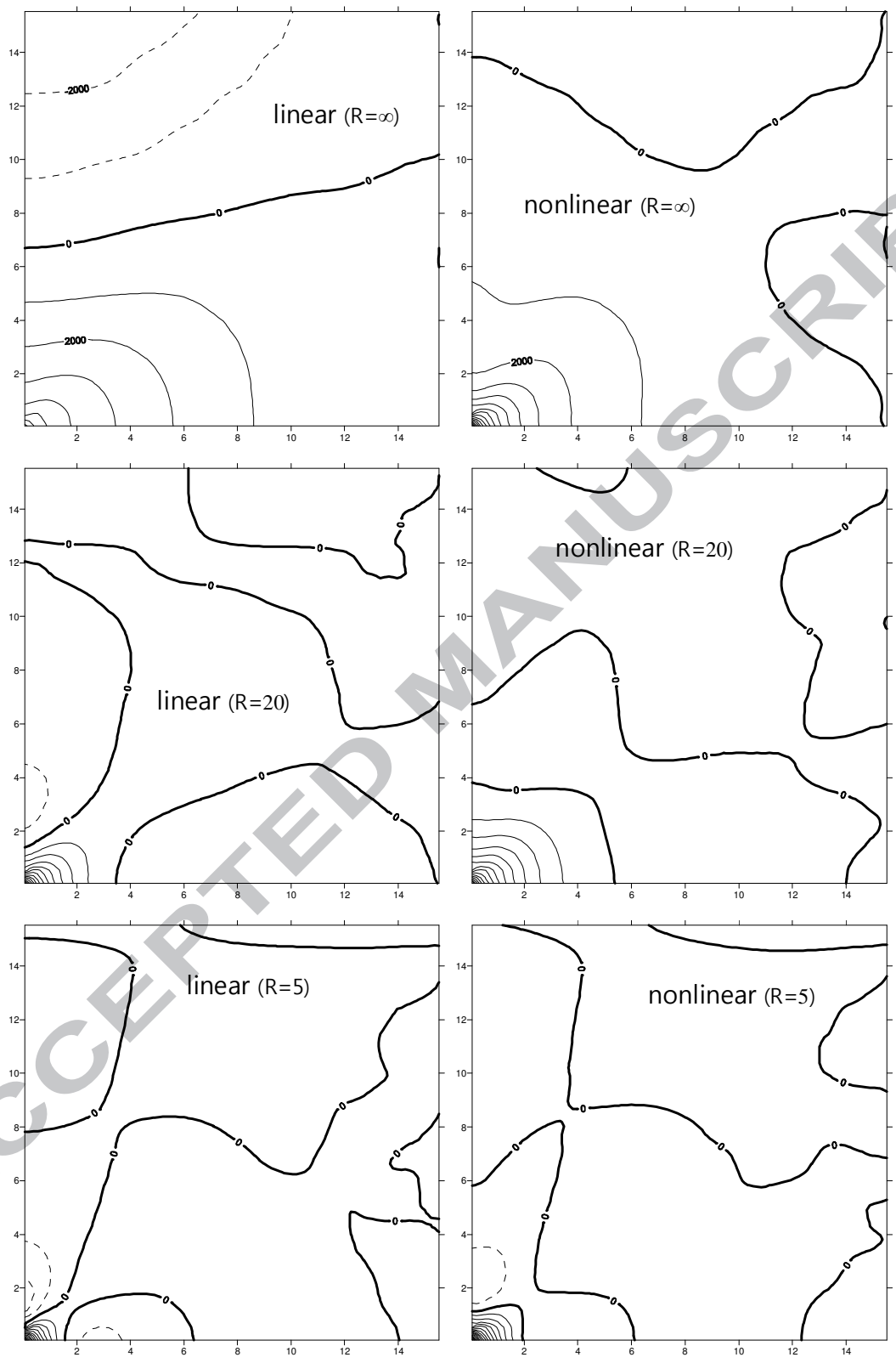

Fig. 8 X_2-directional strain distributions at bottom surface of a quarter part of composite laminated plate/shells.